Crystal structures and magnetization distributions in the field dependent ferromagnetic shape memory alloy $Ni_{54}Fe_{19}Ga_{27}$

2007 J. Phys.: Condens. Matter 19 016201

(http://iopscience.iop.org/0953-8984/19/1/016201)

INSTITUTE OF PHYSICS PUBLISHING JOURNAL OF PHYSICS: CONDENSED MATTER

J. Phys.: Condens. Matter **19** (2007) 016201 (10pp) doi:10.1088/0953-8984/19/1/016201

Crystal structures and magnetization distributions in the field dependent ferromagnetic shape memory alloy $Ni_{54}Fe_{19}Ga_{27}$

P J Brown[1,2], A P Gandy[1], K Ishida[3], R Kainuma[3], T Kanomata[4], H Morito[3], K-U Neumann[1], K Oikawa[3] and K R A Ziebeck[1]

[1] Department of Physics, Loughborough University, LE11 3TU, UK
[2] Institut Laue Langevin, BP 156, 38042 Grenoble, France
[3] Department of Materials Science, Graduate School of Engineering, Tohoku University, Sendai 980-8579, Japan
[4] Faculty of Engineering, Tohoku Gakuin University, Tagajo 985-8537, Japan

Received 4 October 2006, in final form 9 November 2006
Published 7 December 2006
Online at stacks.iop.org/JPhysCM/19/016201

Abstract

The mesoscopic and microscopic mechanisms giving rise to shape memory behaviour in single crystals of the ferromagnetic alloy $Ni_{54}Fe_{19}Ga_{27}$ have been investigated using polarized and unpolarized neutron diffraction. The measurements confirm that the Curie temperature T_C coincides with the martensitic phase transition at $T_M = 296$ K. At room temperature the crystal, as grown, had the tetragonal $L1_0$ structure with $c/a \approx 1.20$. It transformed to the cubic Heusler $L2_1$ structure at ≈330 K. In subsequent heating and cooling cycles the transition took place at $T_M \approx 295$ K and it was found that applying a magnetic field raised T_M by ≈0.3 K T^{-1}, making the material attractive for applications. The tetragonal structure has space group $I4/mmm$ and is related to the cubic parent phase by a Bain transformation. The change in cell volume at the transition is only ≈1%, suggesting that the atomic moments are unchanged, although the magnetization drops significantly. The polarized neutron results show that in the cubic phase the magnetic electrons at the iron-rich sites have predominantly e_g symmetry (60(3)%), a distribution similar to that observed in Fe_3Al and Fe_3Si. A small transfer of magnetization from Fe to Ni is associated with the martensitic transition, but no significant redistribution of magnetic electrons between orbitals whose degeneracy is lifted, such as that predicated by the band Jahn–Teller mechanism, was observed.

(Some figures in this article are in colour only in the electronic version)

1. Introduction

During the past decade smart materials, particularly those exhibiting shape memory behaviour, have received increasing attention because of their great scientific and technological

promise [1]. Shape memory materials can be formed at one temperature T_F, then cooled to a lower temperature T_D and plastically deformed; on re-heating to T_F they will regain their original shape. The change in shape can also produce a force or a combination of force and displacement, which can be exploited in electromechanical devices. The origin of shape memory is a martensitic structural phase transition, which must occur at a temperature T_M intermediate between T_F and T_D; it is therefore usually activated by a change in temperature or applied stress. However, for many applications, particularly in medicine, a change of temperature or pressure is inappropriate. For this reason there is an ongoing search for ferromagnetic materials in which the transition can be induced by a magnetic field at constant temperature. Ni_2MnGa [2], which is the most extensively studied ferromagnetic shape memory compound, is too brittle and its transition temperature T_M too low for convenient use. These deficiencies can be addressed whilst maintaining the shape memory property, either by changing the stoichiometry as in $Ni_{2+x}Mn_{1-x}Ga$ [3], or by substituting other elements, or by a combination of both as in Co–Ni–Ga and Co–Ni–Al [4–10]. In order to maximize the potential of these materials both the martensitic and Curie temperatures T_M and T_C and the magnetization must be optimized. It has been shown that, in this respect, the Ni–Fe–Ga system is promising, and in particular the alloy $Ni_{54}Fe_{19}Ga_{27}$, for which T_C and T_M are nearly coincident, at $\approx$300 K [11–15]. The structure of $Ni_{54}Fe_{19}Ga_{27}$ is reported to be similar to that of Ni_2MnGa in both the austenite and martensite phases [17]. Thus the mesoscopic transformation process in $Ni_{54}Fe_{19}Ga_{27}$ may be expected to be similar to that recently established for Ni_2MnGa, involving two successive shears on {110} planes along $\langle 1\bar{1}0\rangle$ directions [18]. The shape memory property arises from the fixed orientation relationships, determined by this process, between the martensitic twins and the cubic axes of the austenite parent phase. In Ni_2MnGa the structural phase transition is associated with a band Jahn–Teller effect, in which the energy is lowered by redistribution of electrons in bands whose degeneracy is lifted in the transition to the martensitic phase [19]. The present investigation was undertaken to establish whether these microscopic and mesoscopic mechanisms are general features of ferromagnetic shape memory systems and in particular of those with a Heusler parent phase.

1.1. Previous measurements

The Ni–Fe–Ga system has been extensively investigated in attempts to optimize shape memory behaviour in the ferromagnetic state [11–15]. The ternary series is formed from solid solutions of the Fe–Ga and Ni–Ga binary components in which the B2 phase occurs over a wide range of composition. These investigations identified alloys in the series $Ni_{73-x}Fe_xGa_{27}$ with $19 \leqslant x \leqslant 25$ as the most suitable for applications.

Replacing iron by nickel lowers T_C and raises T_M until for $Ni_{54}Fe_{19}Ga_{27}$ they are approximately coincident at 300 K. A schematic phase diagram showing the dependence of T_C and T_M on Fe content x is presented in figure 1. DSC and magnetization measurements [11] on $Ni_{54}Fe_{19}Ga_{27}$ show that the structural transition has a 15 K hysteresis: the associated enthalpy and entropy are 340.28 J mol^{-1} and 1.13 J mol^{-1} K^{-1} respectively. The spontaneous magnetization at 5 K is 55.6 J T^{-1} kg^{-1}, which corresponds to a moment of 2.4 μ_B/Fe. The thermal variation of the spontaneous magnetization and the temperature derivative of the magnetization measured in a field of 5 T are shown in figure 2. The structure of the cubic parent phase is dependent on heat treatment and is one or other of the $L2_1$ (Heusler) or B2 (CsCl) structures. The $L2_1$–B2 order–disorder temperature was found to be 970 K and an annealing temperature of 773 K was used to establish the Heusler structure [20]. $L2_1$ order was confirmed by x-ray diffraction, which gave a lattice parameter $a = 5.740$ Å for $Ni_{54}Fe_{19}Ga_{27}$ at 310 K. Below 300 K the martensitic phase was found to have a structure with a sevenfold

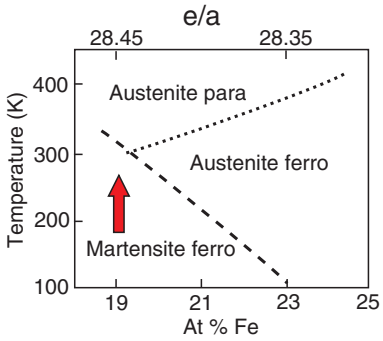

Figure 1. A schematic phase diagram of $Ni_{73-x}Fe_xGa_{27}$ for $19 \leqslant x \leqslant 25$ after [11]. The arrow indicates the composition of the crystal used in the present investigation. To avoid uncertainties in defining the valencies the electron atom ratio e/a has been calculated using the total number of electrons in the constituent atoms.

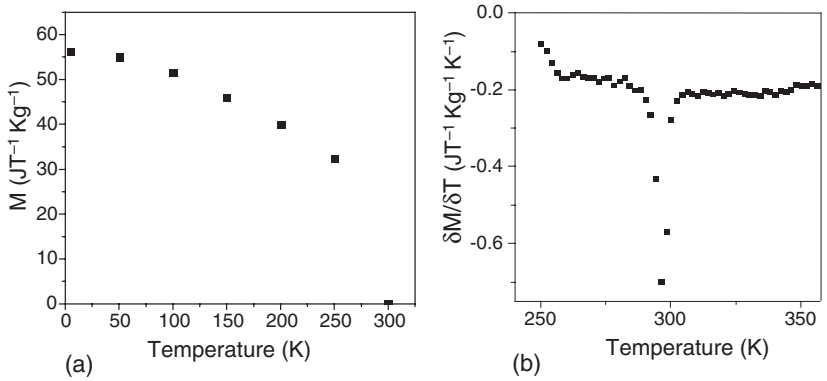

Figure 2. (a) The thermal variation of the spontaneous magnetization M of $Ni_{54}Fe_{19}Ga_{27}$. (b) The derivative of the magnetization with respect to temperature measured in a field of 5 T.

modulation, similar to that found in Ni_2MnGa. The unit cell was reported to be monoclinic with $a = 4.27$ Å, $b = 2.7$ Å, $c = 29.3$ Å and $\beta = 86.6°$ [15]. Under applied stress this sevenfold martensitic structure transformed to a tetragonal $L1_0$ phase with $a = 3.81$ Å and $c = 3.27$ Å [16].

2. Experimental details

2.1. Material

The single crystal used in the present series of experiments was a cube with edge ≈4 mm cut from a larger boule grown by the Bridgman method. The stoichiometry $Ni_{54}Fe_{19}Ga_{27}$ was checked by microprobe analysis and was confirmed by the martensitic transition and ferromagnetic Curie temperatures of 296 K obtained from the magnetization measurements shown in figure 2.

2.2. Unpolarized neutron diffraction

A preliminary investigation of the crystallographic structure was carried out using the four-circle diffractometer D10 at the ILL Grenoble. The neutron wavelength was 1.26 Å and the

crystal was mounted in a four-circle He-flow cryostat. A search at 300 K revealed reflections all of which could be indexed on a tetragonal face centred cell, $a = 5.397(2)$, $c = 6.4897(4)$ Å, $c/a = 1.202$, leading to a conventional body centred tetragonal cell with $a = 3.816(2)$, $c = 6.4897(4)$ Å. This confirmed that at 289 K the crystal was in the martensitic phase. The integrated intensities of all accessible reflections from this unit cell with $\sin\theta/\lambda < 0.75$ Å^{-1} were measured. In addition, long q-scans were made at 289 and 28 K along ⟨110⟩ and ⟨100⟩ directions through four Brillouin zones centred on the {200}, {202}, {440} and {442} reciprocal lattice points, in order to detect any modulation of the structure associated with the martensitic distortion. No significant satellite reflections were found in any of the scans. The tetragonal structure persisted unchanged on warming to 330 K, the maximum temperature permitted in the four-circle cryostat. Finally, the set of reflections that had been measured at 300 K was remeasured at 27 K. The mean structure amplitudes were determined from the integrated intensity measurements by averaging over symmetry equivalents. The final data sets at 298 and 27 K contained respectively 33 and 34 independent reflections.

Further integrated intensity measurements in both the transformed and cubic phases were made using the four-circle hot-source diffractometer D9 at ILL. The crystal was mounted in a resistance furnace compatible with the four-circle geometry, enabling stable temperatures between 298 and 350 K to be attained. The short wavelengths available on D9 together with the multi-detector have been found to be an excellent combination for determining the transformation mechanisms in shape memory compounds [18]. A wavelength of 0.84 Å enables all the twin components into which the fundamental cubic reflections split to be recorded with the multi-detector placed at the 2θ setting of each cubic reflection. Measurements on the $Ni_{54}Fe_{19}Ga_{27}$ crystal in its original form at ambient temperature (298 K) showed that it contained essentially only a single tetragonal martensitic twin domain. The integrated intensities of all accessible reflections with $h \geqslant 0$ and $\sin\theta/\lambda < 1.0$ Å^{-1} were measured at this temperature using a neutron wavelength $\lambda = 0.84$ Å with the crystal in this state. After the polarized neutron measurements described in the next section had been made, the crystal was again mounted on D9 and the same set of integrated intensity measurements was made with the crystal in the cubic phase at 350 K. The integrated intensities measured at both temperatures were averaged over equivalents to obtain a set of 155 and 41 independent reflections for the tetragonal and cubic phases respectively.

A least squares refinement of the tetragonal structure was carried out using the data measured on D10 in which the parameters were a scale factor, a magnetic moment associated with the Fe(A) sites, site scattering lengths and isotropic temperature factors for each of the three independent sites of the tetragonally distorted $L2_1$ structure shown in figure 3. The sum of the site scattering lengths was fixed as 37.3 fm, the value appropriate to one formula unit $Ni_{2.16}Fe_{0.76}Ga_{1.08}$. The results are given in table 1; they are consistent with an ordered $L2_1$ structure in which the excess Ni and Ga atoms occupy the vacant Fe(A) sites. The fit obtained using isotropic temperature factors was markedly improved by allowing them to become anisotropic as indicated in table 1. The increase in both the magnitude and anisotropy of the temperature factors on cooling from 300 to 38 K strongly suggests that they reflect static atomic shifts associated with the martensitic transition, which are greatest in the tetragonal [001] direction and evolve with decreasing temperature.

Further refinements were carried out using the two data sets measured on D9 to allow comparison of the tetragonal and cubic structures. These showed that there was no significant extinction in the intensities at either temperature. They confirmed the site occupation parameters determined from the D10 data. The greater angular extent of the D9 data allowed rather better determination of the temperature factors. The results are given in table 2.

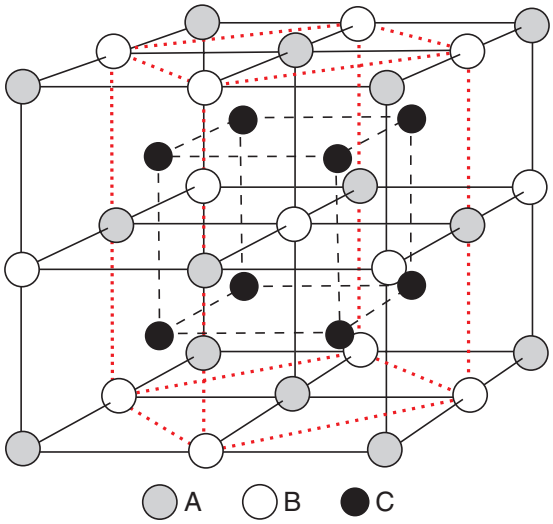

Figure 3. The $L2_1$ Heusler structure of the austenite phase of $Ni_{54}Fe_{19}Ga_{27}$. At the ideal composition Ni_2FeGa the A sites are occupied by Fe, the B sites by Ni and the C sites by Ga. The unit cell of the tetragonal martensite phase which is related to the parent structure through a Bain transformation is shown by the dotted lines.

Table 1. Parameters obtained in least squares refinements of the tetragonal structure of $Ni_{54}Fe_{19}Ga_{27}$.

Site	Position	Parameter	300 K		38 K	
		μ (μ_B)	1.31(21)	1.14(15)	2.28(16)	1.76(13)
		b (fm)	9.3(3)	9.4(2)	9.6(3)	9.6(3)
A	000	B (Å^2)	0.32(16)		0.7(2)	
		B_{11} (Å^2)		0.39(9)		1.0(2)
		B_{33} (Å^2)		0.79(18)		1.8(3)
		b (fm)	7.5(3)	7.4(3)	7.3(4)	7.3(4)
		B (Å^2)	0.32(2)		0.5(3)	
B	$00\frac{1}{2}$	B_{11} (Å^2)		0.39(12)		1.0(2)
		B_{33} (Å^2)		0.5(2)		1.5(4)
		b (fm)	10.3(2)	10.25(15)	10.2(2)	10.2(3)
		B (Å^2)	0.41(13)		0.571(17)	
C	$0\frac{1}{2}\frac{1}{4}$	B_{11} (Å^2)		0.36(8)		0.79(14)
		B_{33} (Å^2)		1.05(15)		1.7(3)
		R (%)	6.0	3.5	6.0	4.1
		χ^2	23	7.5	21	9.5

2.3. Polarized neutron measurements

Polarized neutron flipping ratio measurements were made using the polarized neutron diffractometer D3 located on the hot source at the ILL Grenoble. The crystal, in its tetragonal single-twin state confirmed on D9, was mounted with a $[1\bar{1}0]$ axis vertical in a high temperature insert placed in the 10 T superconducting magnet on the omega table of the diffractometer. The

Table 2. Structure parameters for $Ni_{54}Fe_{19}Ga_{27}$ in the virgin crystal at 298 K and in the cubic phase at 350 K.

	350 K				298 K			
	Space group $Fm\bar{3}m$		$a = 5.774(4)$ Å		Space group $I4/mmm$		$a = 3.818(6)$ Å $c = 6.496(16)$ Å	
Site	Position	b_{site} (fm)	B (Å^2)	μ (μ_B)	Position	b_{site} (fm)	B_{ij}[a]	μ (μ_B)
A	4(a) 000	9.34(12)	0.76(2)	0.48(9)	2(a) 000	9.40(9)	0.52(3) 0.54(3)	0.5(4)
B	4(b) $\frac{1}{2}\frac{1}{2}\frac{1}{2}$	7.46(12)	0.88(3)	0	2(b) $00\frac{1}{2}$	7.20(10)	0.58(4) 0.46(4)	0
C	8(c) $\frac{1}{4}\frac{1}{4}\frac{1}{4}$	10.26(12)	0.94(2)	0	4(d) $0\frac{1}{2}\frac{1}{4}$	10.35(5)	0.54(2) 0.71(2)	0
χ^2	1.8				5.5			
R_{cryst}	1.6				3.8			

[a] For each pair of values the upper is B_{11} and the lower B_{33}, the units are Å^2.

flipping ratios of all accessible independent reflections with $\sin\theta/\lambda < 0.8$ Å^{-1} were measured with $\lambda = 0.84$ Å at 289 K, ensuring that, where possible, two members of each equivalent set were included. The temperature was then raised to 350 K, so that the crystal was in the cubic phase, and the flipping ratios of the same set of reflections were remeasured. After averaging over equivalent reflections, magnetic structure factors were derived from the flipping ratios for both sets of data using nuclear structure factors calculated using the parameters determined from the integrated intensity data. A set of 36 independent structure factors was obtained for the tetragonal phase, which was reduced to 26 by the higher symmetry of the cubic phase.

Finally, the field dependence of the structural phase transition was investigated by measuring the diffracted intensity at the peak position for the cubic 220 reflection on heating and cooling through the martensitic transition in different applied magnetic fields between 0 and 9.6 T. The results obtained for the cooling cycle are shown in figure 4(a). The martensitic transition temperature T_M was estimated from these measurements as the temperature of maximum slope of the intensity versus temperature curves; the values obtained in both heating and cooling cycles are shown in figure 4(b).

3. Analysis of the results

An initial determination of the magnetic moments associated with the different sites of the Heusler alloy structure was made by assigning spherically symmetric Ni^{2+} and Fe^{2+} form factors to the magnetization at the B and A sites respectively. The form factors used were those calculated for the free ions [21]. The results obtained by fitting the moments associated with each of the sites to the measured structure factors are shown in table 3 (model 1). The goodness of fit of the models was assessed by calculating

$$\chi^2 = \left(\sum_{i=N}^{i=1}\left(\frac{F(i)_{obs} - F(i)_{calc}}{\sigma F(i)_{obs}}\right)^2\right) \Big/ \left(N - N_{pars}\right)$$

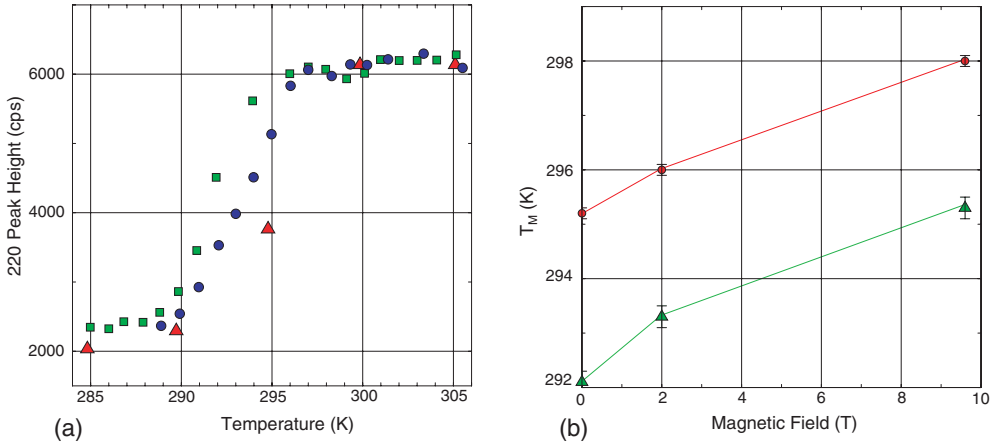

Figure 4. (a) The temperature dependence of the peak height of the 220 reflection of $Ni_{54}Fe_{19}Ga_{27}$ measured while cooling in zero field (squares), 2 T (circles) and 9.6 T (triangles). (b) The martensitic transition temperature T_M in different magnetic fields estimated from the points of maximum slope of the 220 peak height versus temperature curves whilst heating (circles) and cooling (triangles). Lines through the points have been inserted as a guide to the eye.

Table 3. Parameters obtained for different models fitted to the magnetic structure factors of $Ni_{54}Fe_{19}Ga_{27}$ at 350 and 298 K.

		$T = 350$ K				$T = 298$ K		
Model		A	B	C		A	B	C
1	μ (μ_B)	0.673(10)	0.007(9)	0.145(6)		0.89(2)	0.18(2)	0.236(5)
	χ^2		6.3				9.1	
2	μ (μ_B)	0.644(10)	0.002(7)	0.138 (5)		0.85(2)	0.16(2)	0.229(5)
	a_2 (μ_B)	0.12(3)				0.23(6)		
	χ^2		3.6				6.7	
3	μ (μ_B)	0.640(6)	0.002(6)	0.136(3)		0.860(17)	0.166(13)	0.225(4)
	a_2 (μ_B)	0.127(15)				0.19(7)		
	e_g (%)	61(3)		55(10)	$3z^2 - r^2$	32(6)		16(15)
					$x^2 - y^2$	33(13)		27(23)
	t_{2g} (%)	39(3)		45(10)	xy	6(13)		30(23)
					$zx + zy$	28(8)		26(20)
	χ^2		1.0				2.83	

where N is the number of observations and N_{pars} the number of fitted parameters. A slightly more sophisticated model in which the scattering from each site is given by

$$f_a(\mathbf{k}) = a_0\langle j_0\rangle + a_2\langle j_2\rangle \qquad \text{with } \langle j_n\rangle = \int_0^\infty J_n(kr)U(r)\,\mathrm{d}r^3$$

allows some flexibility in the radial magnetization distributions. $J_n(kr)$ is an nth order spherical Bessel function and $U(r)$ is the radial distribution function of the magnetic electrons. The coefficient a_0 gives the atomic magnetic moment. A positive coefficient a_2 corresponds to expansion of the form factor, possibly due to an orbital magnetic moment. A significantly improved fit was obtained with a positive value of a_2 for the A site (table 3 model 2). Finally, the model was extended to allow non-spherical distributions of magnetization around the A and B sites by including spherical harmonic angular modulation of the magnetization distribution

consistent with the site symmetries. In this formulation the scattering factor associated with each site can be written as

$$f_a(\mathbf{k}) = a_0\langle j_0\rangle + a_2\langle j_2\rangle + \sum_{l=2,4}\langle j_l\rangle \sum_{m=-l,l,2} a_{lm} Y_l^m(\hat{\mathbf{k}}).$$

The amplitudes of the spherical harmonics can be directly related to the numbers of unpaired electrons in the different 3d orbitals. For sites with full cubic symmetry the sum over spherical harmonics can be reduced to $\langle j_4\rangle a_4 A(\hat{\mathbf{k}})$, where

$$A(\mathbf{k}) = \frac{3(h^4+k^4+l^4) - 9(h^2k^2+k^2l^2+l^2h^2)}{(h^2+k^2+l^2)^2}$$

and $\gamma = 5(a_4/a_0 + 1)/2$ is the fraction of magnetic electrons in e_g orbitals. The values obtained for the fractions of the unpaired electrons in the different 3d orbitals allowed by the site symmetries at 298 and 350 K are shown in table 3 (model 3).

The most surprising feature of the magnetization distribution is the very significant expansion of the A site form factor represented by the parameter a_2, which is about 20% of the moment value at both temperatures. In the dipole approximation the spectroscopic splitting factor $g = 2/(1-a_2)$; so, if the expansion were due to orbital scattering, it would lead to a ratio $\mu_L/\mu_S \approx 0.25$, which seems unreasonably high. Some of the magnetism at the A site may be due to nickel. If the A site form factor is expressed as a mixture of the Ni^{2+} and Fe^{2+} form factors then it is found that the Ni contribution needs to be approximately twice the Fe part to fit the data. Since the A sites can contain a maximum of 16% of nickel atoms, this would require the nickel atoms to carry an unphysically large moment of about 2.7 μ_B. The results must be interpreted to show that the magnetization distribution around the A site is more compact than that which is found in pure iron, although the reason for this is unclear.

4. Discussion

Bulk magnetization measurements carried out on a polycrystalline sample from the same boule as the crystal used in the present study had already suggested that the structural phase transition could be influenced by an external magnetic field. This is confirmed by the measurements illustrated in figure 4. From these figures it is clear that T_M can be increased by the application of a magnetic field. The rate of increase is approximately 0.3 K T^{-1} between 0 and 9.6 T. This field dependence may be associated with residual stress due to magnetic anisotropy in the tetragonal phase, since it has been shown that the austenite–martensite phase boundary moves to higher temperatures with increasing tensile stress [16]. Residual stress may also explain the significantly higher martensitic start temperature of the virgin, nearly single domain, crystal, which was found to retain the tetragonal structure up to 330 K. In subsequent heating and cooling cycles the transformation from a multi-domain tetragonal form to the cubic structure took place at ≈296 K.

The tetragonal structure of the martensitic phase of $Ni_{54}Fe_{19}Ga_{27}$ is similar to that observed in the $Ni_{2+x}Mn_{1+x}Ga$ system for the composition $Ni_{2.17}Mn_{0.83}Ga$ at which T_M and T_C are again coincident just above room temperature [22]. However, in this latter system the transformation from the cubic to tetragonal structures takes place via an intermediate orthorhombic structure not related to either by a Bain transformation. Although the martensitic phase of $Ni_{54}Fe_{19}Ga_{27}$ studied in the present experiment is tetragonal, an orthorhombic structure has been found at other compositions in the Ni–Fe–Ga system [25]. It is possible that the tetragonal structure is only stable in crystals under strain [16].

In $Ni_{54}Fe_{19}Ga_{27}$, as in other Heusler systems, a martensitic phase transition occurs when the electron concentration is close to $e/a \approx 28$, the value for Ni_2MnGa. In the series

$Ni_{73-x}Fe_xGa_{27}$ with $19 \leqslant x \leqslant 25$ e/a varies from 28.43 to 28.31 and both T_M and T_C depend sensitively on composition. As the Fe concentration increases the martensitic phase is increasingly suppressed: T_M drops by 200 K for a reduction in e/a of 0.1. The Curie temperature T_C on the other hand increases by almost 100 K over the same range of electron concentration.

In the cubic phase the fraction γ of magnetic electrons in orbitals with e_g symmetry is 0.60(3) at the A site and 0.55(10) at the C sites. The A site value is significantly greater than that found for Ni_2MnGa in which Mn occupies the A sites. It is very close to the values found at the equivalent Fe sites in Fe_3Al [23] and Fe_3Si [24], although no significant expansion of the radial form-factors was observed in these alloys. The e_g occupancy at the A sites is not significantly altered in the transition to the tetragonal phase, although the ratio between the moments on the A and C sites decreases and a moment is stabilized at the B sites. There is no really significant redistribution of magnetic electrons between those orbitals whose degeneracy is broken by the transition, although there is an indication that the t_{2g} electrons at the A site favour the zx and zy orbitals whereas those at the C sites prefer the xy orbitals. The band Jahn–Teller effect, which is thought to be important in driving the martensitic transformation in Ni_2MnGa, results from narrowing of bands derived from orbitals which overlap in the direction of crystal elongation and broadening of those which overlap in the direction of compression. The total energy can be reduced by transfer of electrons from the narrowed to the broadened bands. In Ni_2MnGa, with $c/a < 1$, electrons were found to favour the $3z^2 - r^2$ and $xz \pm yz$ sub-bands, in accordance with this mechanism. For $Ni_{54}Fe_{19}Ga_{27}$, with $c/a > 1$, the reverse should be true, but this effect is not evident in our results, which suggests that the band Jahn–Teller mechanism cannot be so important in $Ni_{54}Fe_{19}Ga_{27}$. It may be noted that in both $Ni_{54}Fe_{19}Ga_{27}$ and Ni_2MnGa the martensitic transition leads to a transfer of magnetic electrons from atoms on the A sites to those on the C sites.

The present results show that distortion of the unit cell in the transition is one of the largest yet found in ferromagnetic shape memory alloys. The cell parameters change from $a_{cub} = 5.774$ Å to $a_{tet} = 5.397$, $c_{tet} = 6.4897$ Å, for the fcc tetragonal cell, giving $c/a = 1.202$. Furthermore, above the martensitic start temperature the material is reported to have superelastic properties [16]. These characteristics, together with the improved ductility and the possibility of raising the martensitic phase transition by applying a magnetic field, make the material very promising for applications.

References

[1] Planes A, Manosa L and Saxena A (ed) 2005 *Magnetism and Structure in Functional Materials* (Berlin: Springer)
[2] Webster P J, Ziebeck K R A, Town S L and Peak M S 1984 *Phil. Mag.* **49** 295
[3] Vasilev A N, Bozhko A D, Khovailo V V, Dikshtein I E, Shavrov V G, Buchelnikov V D, Matsumoto M, Suzuki S, Takagi T and Tani J 1999 *Phys. Rev.* B **59** 1113
[4] Sato M, Okazaki T, Furuya Y and Wuttig M 2003 *Mater. Trans. JIM* **44** 372
[5] Brown P J, Ishida K, Kainuma R, Kanomata T, Neumann K-U, Oikawa K, Ouladdiaf B and Ziebeck K R A 2005 *J. Phys.: Condens. Matter* **17** 1301
[6] Oikawa K, Omori T, Sutou Y, Kainuma R and Ishida K 2003 *J. Physique* IV **112** 1017
[7] Chernenko V A, Pons J, Cesari E and Zasimchuk J K 2004 *Scr. Mater.* **50** 225
[8] Oikawa K, Ota T, Gejima F, Ohmori T, Kainuma R and Ishida K 2001 *Mater. Trans. JIM* **42** 2472
[9] Oikawa K, Wulff L, Iijima T, Gejima F, Ohmori T, Fujita A, Fukamichi K, Kainuma R and Ishida K 2001 *Appl. Phys. Lett.* **79** 3290
[10] Wuttig M, Li J and Cracuinescu C 2002 *Scr. Mater.* **44** 2393
[11] Oikawa K, Ota T, Ohmori T, Tanaka Y, Morito H, Fujita A, Kainuma R, Fukamichi K and Ishida K 2002 *Appl. Phys. Lett.* **81** 5201
[12] Murakami Y, Shindo D, Oikawa K, Kainuma R and Ishida K 2003 *Appl. Phys. Lett.* **82** 3695

[13] Oikawa K, Ota T, Sutou Y, Ohmori T, Kainuma R and Ishida K 2002 *Mater. Trans. JIM* **43** 2360
[14] Morito H, Fujita A, Fukamichi K, Ota T, Kainuma R, Ishida K and Oikawa K 2003 *Mater. Trans. JIM* **44** 1
[15] Morito H, Fujita A, Fukamichi K, Kainuma R, Ishida K and Oikawa K 2003 *Appl. Phys. Lett.* **83** 4993
[16] Sutou Y, Kamiya N, Omori T, Kainuma R and Ishida K 2004 *Appl. Phys. Lett.* **84** 1275
[17] Brown P J, Crangle J, Kanomata T, Matsumoto M, Ouladdiaf B, Neumann K-U and Ziebeck K R A 2002 *J. Phys.: Condens. Matter* **14** 10159
[18] Brown P J, Dennis B, Crangle J, Kanomata T, Matsumoto M, Neumann K-U, Justham L M and Ziebeck K R A 2004 *J. Phys.: Condens. Matter* **16** 65
[19] Brown P J, Bargawi A Y, Crangle J, Neumann K-U and Ziebeck K R A 1999 *J. Phys.: Condens. Matter* **11** 4715
[20] Oikawa K, Omori T, Kainuma R and Ishida K 2004 *J. Magn. Magn. Mater.* **272** 2043
[21] Watson R E and Freeman A J 1961 *Acta Crystallogr.* **14** 27
[22] Fröhlich K, Dennis B, Kanomata K, Matsumoto M, Neumann K-U and Ziebeck K R A 2005 *Int. J. Appl. Electron. Mech.* **21** 159
[23] Pickart S J and Nathans R 1961 *Phys. Rev.* **123** 1163
[24] Moss J and Brown P J 1972 *J. Phys. F: Met. Phys.* **2** 358
[25] Ziebeck K R A *et al* 2005 *Report on ILL Experiment* 5-41-337 http://club.ill.fr/cv/